Multi-Frequency ESR Study of the Polycrystalline Phenoxyl Radical of α-(3,5-Di-*tert*-butyl-4-hydroxyphenyl)-*N*-*tert*-butylnitrone in the Diamagnetic Matrix

Toshiki Yamaji,*,† Yohei Noda,† Seigo Yamauchi,‡ and Jun Yamauchi†

Department of Chemistry, Graduate School of Science, Kyoto University, Nihonmatsu-cho, Yoshida, Kyoto 606-8501, Japan, and Institute of Multidisciplinary, Research for Advanced Materials, Tohoku University, Katahira 2-1-1, Aoba-ku, Sendai 980-8577, Japan

Received: August 5, 2005; In Final Form: November 9, 2005

Multifrequency (X-, Q-, and W-band) electron spin resonance (ESR) spectroscopy has been used to characterize the phenoxyl radical produced from α-(3,5-di-*tert*-butyl-4-hydroxyphenyl)-*N*-*tert*-butylnitrone, which is a new spin-trapping reagent. The X-band measurement did not resolve the powder-pattern ESR spectrum. Because of its higher resolution with *g* value, the Q-band ESR study revealed that the *g* factor has an axial-like symmetry and that the observed hyperfine structure in the *Z*-direction is caused by the nitrogen nucleus at the para-position. Furthermore, the results of the W-band ESR experiment more clearly distinguished the perpendicular components from the parallel component, resolving the perpendicular components into *x* and *y* components. The X-band powder spectrum was similar to the X-band ESR spectrum of the radical in a frozen solution of toluene. The computer simulation spectra performed using the obtained parameters fitted the experimental spectra well. A comparison of the amplitude of $g_\perp(g_x, g_y)$ with that of g_z showed that the unpaired electron is delocalized over the π-conjugated framework. Considering the hyperfine coupling constant, it was concluded that about 16% of the unpaired electron distributed over the nitrogen nucleus at the para-position. This study thus showed the significant potential of a multifrequency ESR approach to a powder sample radical in terms of its high resolution with *g* value.

Introduction

Over the past 2 decades, the spin-trapping technique has become a popular tool for the detection and study of a variety of short-lived free radicals that could not have been observed directly by continuous-wave (CW) electron spin resonance (ESR) spectroscopy. In spin-trapping experiments, a free radical reacts with a spin trap, that is, an ESR-silent diamagnetic compound, to form a generated stable free radical, a spin adduct, that can be easily detected by ESR.[1] The spin-trapping technique has been applicable to detect short-lived radicals, e.g., hydroxy and superoxide radicals at low concentrations.[2] These experiments are usually carried out with CW ESR spectroscopy at the conventional frequency, 9.5 GHz (X-band), because of the good sensitivity in concentration (10^{-6}−10^{-7} M) and widespread availability of X-band facilities.

Pacifici and Browning first reported a novel probe, α-(3,5-di-*tert*-butyl-4-hydroxyphenyl)-*N*-*tert*-butylnitrone, which is characteristic in the differentiation between oxy radicals and carbon radicals in spin-trapping reactions (shown in Scheme 1) with a CW X-band ESR spectrum of the phenoxyl radical.[3] The short-lived oxy radicals abstract the phenolic hydrogen of the nitrone **I** to produce the stable phenoxyl radical **II**, whereas the short-lived carbon radicals preferentially add to the α carbon of the nitrone **I** to yield a stable nitroxide **III**. This reaction mechanism shows that the reaction with the nitrone **I** will distinguish between short-lived oxy radicals and carbon radicals.

Through CW X-band ESR research on the phenoxyl radical in a solution, the isotropic *g* value and hyperfine splitting constants of *m*-H, and H and N at the para-position were resolved in the literature[3] as well as in the present work. However, these ESR parameters should be confirmed by the analysis of *g*-tensors or hyperfine tensors, and those anisotropic ESR parameters are required for the study of molecular structure.

SCHEME 1: Spin-Trapping Scheme of α-(3,5-di-*tert*-butyl-4-hydroxyphenyl)-N-*tert*-butylnitrone

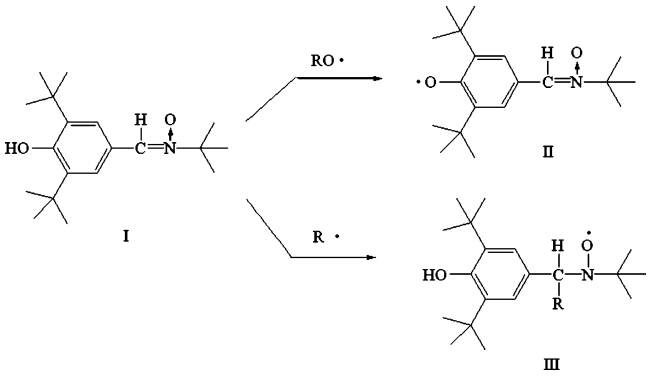

First of all, for the anisotropic spectral analysis, the CW X-band spectra of the phenoxyl radical in the toluene frozen solution were measured. However, anisotropic spectral analysis was impossible on the X-band because many anisotropic peaks overlapped due to the small difference of the components of the *g*-tensors. Second, the polycrystalline phenoxyl radical in a diamagnetic crystal was produced, and the CW ESR was carried out. A powder-pattern similar to the frozen solution spectrum was observed, as expected. As is clear, higher-frequency ESR measurements were essential to clarify the anisotropic ESR parameters.

* Corresponding author. Telephone: +81-75-753-2888. Fax: +81-75-753-6694. E-mail: toshiki-y@nirvana.mbox.media.kyoto-u.ac.jp.
† Kyoto University.
‡ Tohoku University.

10.1021/jp054358z CCC: $33.50
Published on Web 12/27/2005

SCHEME 2: Oxidation Scheme of the Sample

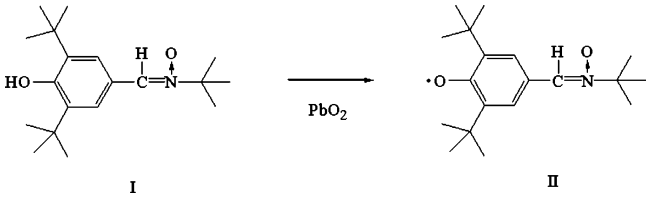

Historically, most commercial spectrometers have always operated around 10 GHz at magnetic fields around 0.3 T using electromagnets. However, over the last 10 years, there has been an increasing interest in achieving the ability to make multifrequency measurements at much larger magnetic fields using superconducting magnets.[4−17] A higher-frequency operation potentially offers much greater absolute sensitivity as well as higher *g*-factor resolution. More generally, multifrequency measurements often allow the field-dependent and field-independent terms of the spin Hamiltonian to be separated and characterized. In this paper, using a multifrequency ESR technique, we characterize the polycrystalline phenoxyl radical generated from α-(3,5-di-*tert*-butyl-4-hydroxyphenyl)-*N*-*tert*-butylnitrone,[18] which is a new spin-trapping reagent, by oxidation with PbO_2.

Materials and Methods

The new spin-trapping reagent, α-(3,5-di-*tert*-butyl-4-hydroxyphenyl)-*N*-*tert*-butylnitrone (**I**), was synthesized following the procedure described in the literature.[3] **I** was oxidized in toluene solution in a vacuum at room temperature (shown in Scheme 2). The produced phenoxyl radical (**II**) was diluted in a diamagnetic crystal, the primary nitrone **I**, with a molar ratio of 1/10. Finally, it was sealed in a 5 mm φESR sample tube in a vacuum.

Experimental and Simulations

X- and Q-band ESR experiments were carried out using JEOL FE1XG and JEOL FE-3X ESR spectrometers, respectively. The W-band ESR measurement was performed using a Bruker W-band ESR spectrometer at Tohoku University. The computer simulations of the ESR spectra were conducted using Bruker Simfonia V.1.25 (shareware).[24]

Results of ESR Spectra and Simulations

The CW X-band ESR spectrum of **II** in a toluene solution from room temperature to 123 K and the polycrystalline **II** spectra in a diamagnetic crystal are shown in Figures 1 and 2a, respectively. As expected, the powder spectra are very similar to the frozen solution spectrum.

As in Figure 2a, it is very difficult or impossible to analyze the ESR powder spectrum of the sample only through the result of the X-band ESR measurement. Thus, a Q-band ESR measurement was subsequently performed. The Q-band ESR spectrum obtained is shown in Figure 3a. Because of the higher resolution with a *g* value about four times that obtained through X-band ESR spectroscopy, the Q-band ESR spectrum enabled

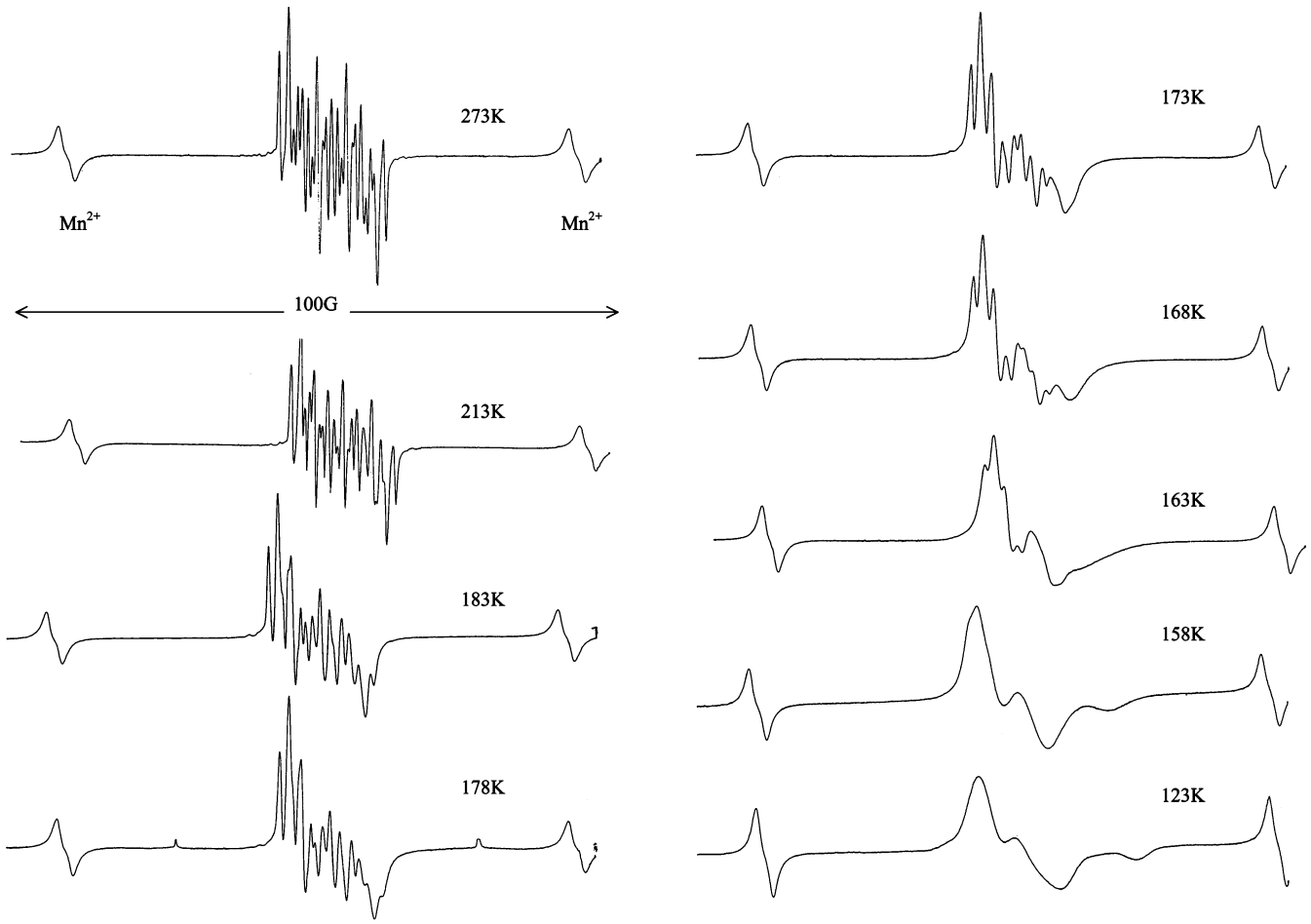

Figure 1. X-band ESR spectra of **II** in toluene solution from room temperature to 123 K. Experimental conditions: microwave frequency, 9.171 GHz; center field, 3280 G; modulation amplitude, 0.5 G; modulation frequency, 100 kHz; microwave power, 1 mW.

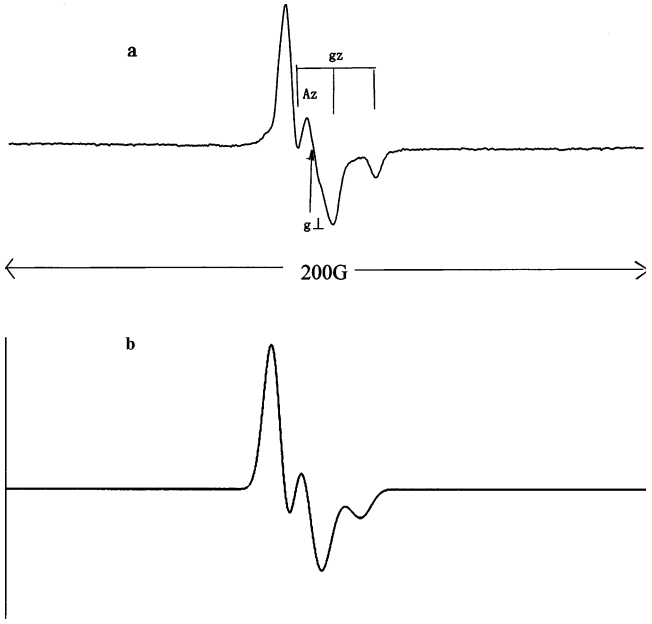

Figure 2. Experimental (a) and simulated (b) X-band ESR powder spectrum of **II**. Experimental conditions: room temperature; microwave frequency, 9.44 GHz; center field, 3370 G; modulation amplitude, 1 G; modulation frequency, 100 kHz; microwave power, 1 mW.

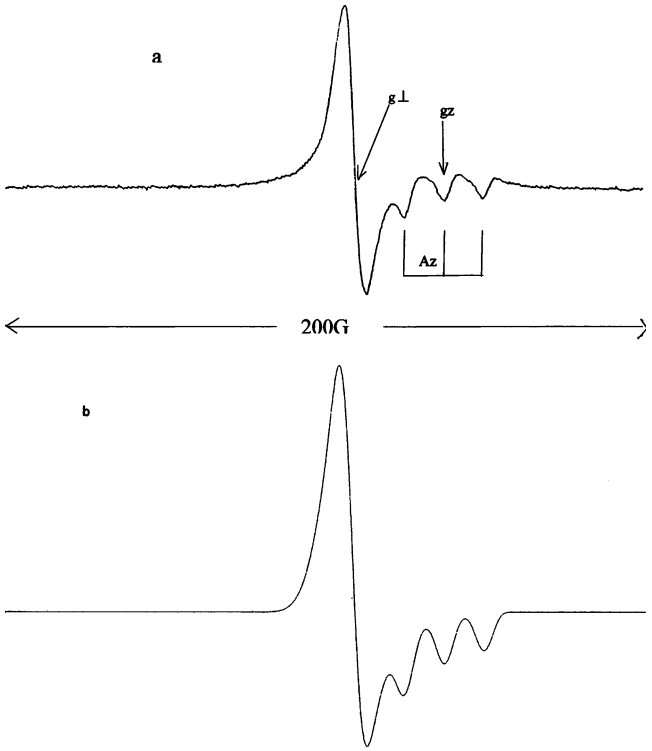

Figure 3. Experimental (a) and simulated (b) Q-band ESR powder spectrum of **II**. Experimental conditions: room temperature; microwave frequency, 35.86 GHz; center field, 12760 G; modulation amplitude, 10 G; modulation frequency, 100 kHz; microwave power, 1.5 mW.

us to analyze the powder-pattern ESR spectrum that was unresolved in the X-band measurement. Figure 3a shows that the *g*-factor has axial-like symmetry and that the observed hyperfine structure consists of three equivalent peaks. As is discussed in the following section, these peaks were assumed to be caused by the nitrogen nucleus at the para-position and are the parallel components of the electron-nitrogen nuclear hyperfine interaction. In addition, because of the higher resolution with a *g* value about two and a half times that obtained

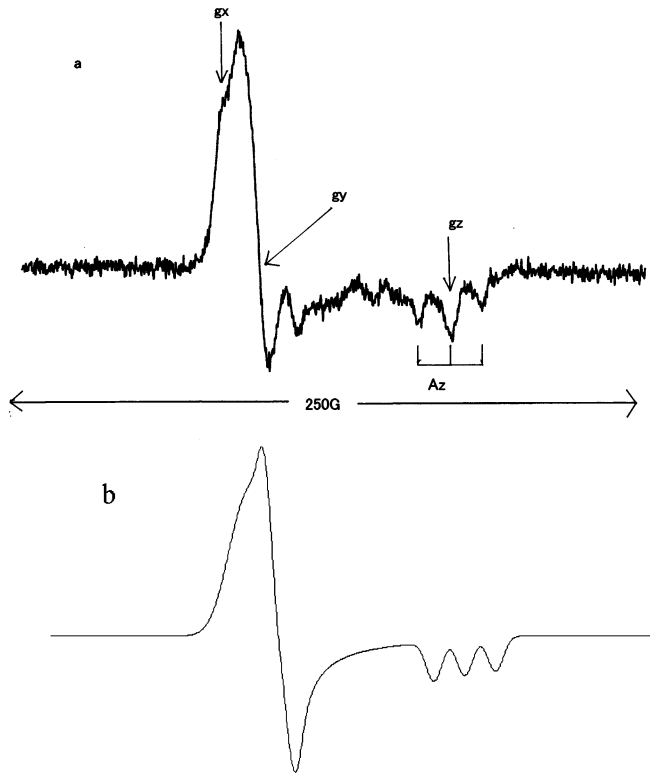

Figure 4. Experimental (a) and simulated (b) W-band ESR powder spectrum of **II**. Experimental conditions: room temperature; microwave frequency, 93.642789 GHz; center field, 33371.5 G; modulation amplitude, 5 G; modulation frequency, 100 kHz; microwave power, 0.04 mW.

through Q-band ESR spectroscopy, the W-band ESR results more clearly distinguished between the perpendicular and parallel components of the spectral peak (shown in Figure 4a) and resolved the perpendicular components into *x* and *y* components.

Finally, to confirm the experimental data, computer simulations of the ESR spectra were carried out using the ESR parameters obtained from the W-band ESR study and the X-band ESR measurement on the radical in a toluene solution at room temperature. X-, Q-, and W-band ESR simulation spectra are shown in Figures 2b, 3b, and 4b, respectively.[24]

Discussion

The W-band ESR study enabled us to analyze the ESR powder spectra of **II** generated from **I** that was unresolved by the X-band ESR investigation. It was revealed that the powder-pattern spectra consist of peaks from the perpendicular (*x*, *y*) and parallel (*z*) components with the parallel splitting of the hyperfine structure caused by the nitrogen nucleus at the para-position. As seeing the W-band experimental spectrum, there are other peaks between the perpendicular region and the high field *g*-feature. In additional investigations, it is concluded that they come from the crystal part that has not been fully grinded, comparing the spectrum not grinded with that grinded in the same way as the present work. Thus, it may be concluded that peaks from a very small amount of crystal part that cannot fully be powdered appear noticeably in a W-band spectrum or higher-frequency ESR data. These conclusions appear to be applicable to a series of the phenoxyl radicals in our study.[19]

On the other hand, the isotropic ESR parameters had been obtained by the X-band ESR measurement of **II** in toluene solution. The ESR data obtained from the W-band ESR powder study and the X-band ESR solution spectrum are summarized

TABLE 1: ESR Parameters Obtained from W-Band ESR Powder Spectrum and X-Band ESR Solution Measurement

g_x	g_y	g_z	g_{ave}	g_{iso}	$A_{N,\perp}$ (G)	$A_{N,\parallel}$	$A_{N,iso}$	$A_{p-H,iso}$	$A_{m-H,iso}$
2.007 45	2.006 60	2.002 12	2.005 39	2.006	1.57	12.35	5.16	2.66	1.54
							5.05[a]	2.60[a]	1.50 (or 1.70)[a]

[a] Reference 3.

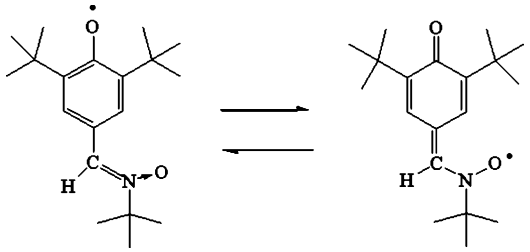

Figure 5. Resonance structure of **II**.

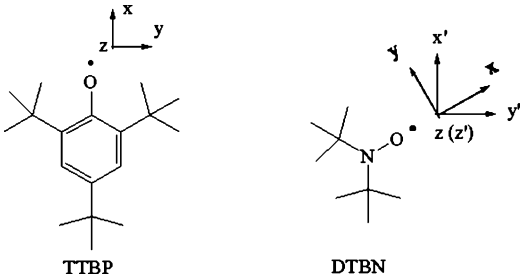

Figure 6. Molecular structures and the principal axes of TTBP and DTBN. The calculated spin densities on the oxygen atom of each radicals are 0.365815 (TTBP), 0.521473 (DTBN), respectively. *g*-tensors are (g_x,g_y,g_z) = (2.00718, 2.00428, 2.00239) (TTBP),[21] (2.00872, 2.00616, 2.00270) (DTBN).[22]

in Table 1. g_{av} was calculated using eq 1.

$$g_{av} = \frac{1}{3}(g_x + g_y + g_z) \quad (1)$$

The perpendicular component of the hyperfine structure with the para-nitrogen nucleus is not visible, disappearing in the line width. Therefore, $A_\perp (= A_{N,i}\ (i = x, y))$ was calculated following eq 2.

$$A_{N,\perp} = \frac{1}{2}(3A_{N,iso} - A_{N,z}) \quad (2)$$

As shown in Figures 2b, 3b, and 4b, the computer-simulated X-, Q-, and W-band ESR spectra obtained using these ESR parameters result in a good fit to the experimental spectra. As shown in Table 1

$$g_\perp(g_x,g_y) > g_z \quad (3)$$

therefore, the unpaired electron is delocalized over the π-conjugated framework. In addition, considering the magnitude of $A_{N,z}$, it was revealed that the density of the unpaired electron is distributed over the nitrogen nucleus at the para-position.

The radical structure was calculated using the Gaussian03 program[20] to estimate the isotropic hyperfine splitting constants and spin density at the nitrogen nucleus. The structure of the radical was optimized, and the parameters were calculated. The B3LYP method and the 6-31G(d) basis set were used for these calculations. The obtained spin density was 0.1999, giving the isotropic hyperfine coupling constant 4.341 G. Consequently, the validity of this experimental study was confirmed by the quantum chemical calculation.

g-tensors were analyzed in terms of the resonance structure of **II**. The resonance structure of **II** is shown in Figure 5. In terms of the resonance structure, it may be assumed that the *g*-tensors of **II** are estimated as the superposition of those of a phenoxyl and a nitroxy radical. For the qualitative calculation, the 2,4,6-tri-*tert*-butyl phenoxyl radical (TTBP) and di-*tert*-butyl nitroxy radical (DTBN) were chosen as model phenoxyl and nitroxy radicals, respectively. The molecular structures and principal axes of these radicals are shown in Figure 6. The structures of these radicals were optimized, and the spin densities on the oxygen atom of these radicals were obtained using the Gaussian98 program.[21] The B3LYP method and the 6-31G(d) basis set were used for these calculations. The *g*-tensors of these radicals are referred to in the literature.[22,23] The coordinate transforms for the *g*-tensors of DTBN are given by

$$g_{DTBN,i'} = \sqrt{{g_{DTBN,x}}^2 \sin^2\theta + {g_{DTBN,y}}^2 \cos^2\theta}\ (i' = x', y') \quad (4)$$

$$g_{DTBN,z'} = g_{DTBN,z} \quad (5)$$

with angle θ between the *y*-axis and the *i*′-axis. Consequently, $g_{DTBN,x'}$ ($\theta = 30°$) and $g_{DTBN,y'}$ ($\theta = 120°$) are 2.00680 and 2.0088, respectively.

As a result, the *g*-tensors can be calculated by the following equations, eqs 6−8.

$$a = \frac{\text{spin density on phenoric oxygen atom of } \mathbf{II}}{\text{spin density on oxygen atom of TTBP}} \quad (6)$$

$$b = \frac{\text{spin density on } p\text{-oxygen atom of } \mathbf{II}}{\text{spin density on oxygen atom of DTBN}} \quad (7)$$

$$g_{cal,i} = \frac{ag_{TTBP,i} + bg_{DTBN,i'}}{a + b}\ ((i,i') = (x,x'), (y,y'), (z,z')) \quad (8)$$

The calculation results are $g_{cal,x} = 2.00700$, $g_{cal,y} = 2.00612$, $g_{cal,z} = 2.00254$, and $g_{cal,av} = 2.00522$ and are in good agreement with the experimental data, confirming the analysis result of this study.

Conclusions

The multifrequency ESR technique enabled us to analyze the powder-pattern ESR spectra of the phenoxyl radical derivative generated from a novel probe, α-(3,5-di-*tert*-butyl-4-hydroxy phenyl)-*N*-*tert*-butylnitrone; as a result, we were able to characterize the new spin-trapping substitute in terms of the ESR parameters, confirming the electronic structure of the phenoxyl radical. This study thus shows the significant potential of a multifrequency ESR approach to powder sample radicals, in particular, samples that are difficult to be acquired as single crystal, in terms of a high resolution with *g* value.

Acknowledgment. We thank the Academic Center for Computing and Media Studies, Kyoto University, and Mr. Yoshiaki Ozawa for the Gaussian program.

Supporting Information Available: Supporting Figure 1, X-band powder-pattern ESR spectrum of the phenoxyl radical derivative generated from a novel probe, α-(3,5-di-*tert*-butyl-4-hydroxyphenyl)-*N*-*tert*-butylnitrone, Supporting Figure 2, Q-band powder-pattern ESR spectrum of the phenoxyl radical derivative generated from a novel probe, α-(3,5-di-*tert*-butyl-4-hydroxyphenyl)-*N*-*tert*-butylnitrone, and Supporting Figure 3, W-band powder-pattern ESR spectrum of the phenoxyl radical derivative generated from a novel probe, α-(3,5-di-*tert*-butyl-4-hydroxyphenyl)-*N*-*tert*-butylnitrone. This material is available free of charge via the Internet at http://pubs.acs.org.

References and Notes

(1) Degray, J. A.; Mason, R. P. Biological Spin Trappings. In *Electron Spin Resonance*; The Royal Society of Chemistry: Cambridge, U.K., 1994; Vol. 14, Chapter 8, pp 246−301.

(2) Janzen, E. G. In *Free Radicals in Biology*; Pryor, W. A., Ed.; Academic Press: New York, 1980; Vol. 4, p 115.

(3) Pacifici, J. G.; Browning, H. L., Jr. *J. Am. Chem. Soc.* **1970**, *92*, 5231−5233.

(4) Janzen, E. G.; Blackburn, B. J. *J. Am. Chem. Soc.* **1968**, *90*, 5909−5910.

(5) Chalfont, G. R. Perkins, M. J.; Horsfield, A. *J. Am. Chem. Soc.* **1968**, *90*, 7141−7142.

(6) Janzen, E. G.; Gerlock, J. L. *J. Am. Chem. Soc.* **1969**, *91*, 3108−3109.

(7) Janzen, E. G.; Blackburn, B. J. *J. Am. Chem. Soc.* **1969**, *91*, 4481−4490.

(8) Birrell, G. B.; Van, S. P.; Griffith, O. H. *J. Am. Chem. Soc.* **1973**, *95*, 2451−2458.

(9) Lou, Y.; Ge, M.; Freed, J. H. *J. Phys. Chem. B* **2001**, *105*, 11053−11056.

(10) Link, G.; Berthold, T.; Bechtold, M.; Weidner, J.-U.; Ohmes, E.; Tang, J.; Poluektov, O.; Utschig, L.; Schlesselman, S. L.; Thurnauer, M. C.; Kothe, G. *J. Am. Chem. Soc.* **2001**, *123*, 4211−4222.

(11) Pogni, R.; Lunga, G. D.; Basosi, R. *J. Am. Chem. Soc.* **1993**, *115*, 1546−1550.

(12) Smirnova, T. I.; Smirnov, A. I.; Clarkson, R. B.; Belford, R. L.; Kotake, Y.; Janzen, E. G. *J. Phys. Chem. B* **1997**, *101*, 3877−3885.

(13) Barra, A. L.; Brunel, L. C.; Robert, J. B. *Chem. Phys. Lett.* **1990**, *175*, 621−623.

(14) Krinichnyi, V. I.; Konkin, A. L.; Devasagayam, P.; Monkman, A. P. *Synth. Met.* **2001**, *119*, 281−282.

(15) Frantz, S.; Hartmann, H.; Doslik, N.; Wanner, M.; Kaim, W.; Kummerer, H.-J.; Denninger, G.; Barra, A.-L.; Duboc-Toia, C.; Fiedler, J.; Ciofini, I.; Urban, C.; Kaupp, M. *J. Am. Chem. Soc.* **2002**, *124*, 10563−10571.

(16) Prisner, T.; Lyubenova, S.; Atabay, Y.; MacMillan, F.; Kroger, A.; Klimmek, O. *J. Biol. Inorg. Chem.* **2003**, *8*, 419−426.

(17) Ivancich, A.; Dorlet, P.; Goodin, D. B.; Un, S. *J. Am. Chem. Soc.* **2001**, *123*, 5050−5058.

(18) Barclay, L. R. C.; Vinqvist, M. R. *Free Radical Biol. Med.* **2000**, 28, 1079−1090.

(19) Yamaji, T.; Baba, M.; Islam, SM. S.; Yamauchi, S.; Yamauchi, J. In preparation.

(20) Frisch, M. J.; Trucks, G. W.; Schlegel, H. B.; Scuseria, G. E.; Robb, M. A.; Cheeseman, J. R.; Montgomery, J. A., Jr.; Vreven, T.; Kudin, K. N.; Burant, J. C.; Millam, J. M.; Iyengar, S. S.; Tomasi, J.; Barone, V.; Mennucci, B.; Cossi, M.; Scalmani, G.; Rega, N.; Petersson, G. A.; Nakatsuji, H.; Hada, M.; Ehara, M.; Toyota, K.; Fukuda, R.; Hasegawa, J.; Ishida, M.; Nakajima, T.; Honda, Y.; Kitao, O.; Nakai, H.; Klene, M.; Li, X.; Knox, J. E.; Hratchian, H. P.; Cross, J. B.; Adamo, C.; Jaramillo, J.; Gomperts, R.; Stratmann, R. E.; Yazyev, O.; Austin, A. J.; Cammi, R.; Pomelli, C.; Ochterski, J. W.; Ayala, P. Y.; Morokuma, K.; Voth, G. A.; Salvador, P.; Dannenberg, J. J.; Zakrzewski, V. G.; Dapprich, S.; Daniels, A. D.; Strain, M. C.; Farkas, O.; Malick, D. K.; Rabuck, A. D.; Raghavachari, K.; Foresman, J. B.; Ortiz, J. V.; Cui, Q.; Baboul, A. G.; Clifford, S.; Cioslowski, J.; Stefanov, B. B.; Liu, G.; Liashenko, A.; Piskorz, P.; Komaromi, I.; Martin, R. L.; Fox, D. J.; Keith, T.; Al-Laham, M. A.; Peng, C. Y.; Nanayakkara, A.; Challacombe, M.; Gill, P. M. W.; Johnson, B.; Chen, W.; Wong, M. W.; Gonzalez, C.; Pople, J. A. *Gaussian 03*, revision C.02; Gaussian, Inc.: Wallingford CT, 2004.

(21) Frisch, M. J.; Trucks, G. W.; Schlegel, H. B.; Scuseria, G. E.; Robb, M. A.; Cheeseman, J. R.; Zakrzewski, V. G.; Montgomery, J. A., Jr.; Stratmann, R. E.; Burant, J. C.; Dapprich, S.; Millam, J. M.; Daniels, A. D.; Kudin, K. N.; Strain, M. C.; Farkas, O.; Tomasi, J.; Barone, V.; Cossi, M.; Cammi, R.; Mennucci, B. Pomelli, C.; Adamo, C.; Clifford, S.; Ochterski, J.; Petersson, G. A.; Ayala, P. Y.; Cui, Q.; Morokuma, K.; Salvador, P.; Dannenberg, J. J.; Malick, D. K.; Rabuck, A. D.; Raghavachari, K.; Foresman, J. B.; Cioslowski, J.; Ortiz, J. V.; Baboul, A. G.; Stefanov, B. B.; Liu, G.; Liashenko, A.; Piskorz, P.; Komaromi, I.; Gomperts, R.; Martin, R. L.; Fox, D. J.; Keith, T.; Al-Laham, M. A.; Peng, C. Y.; Nanayakkara, A.; Challacombe, M.; Gill, P. M. W.; Johnson, B.; Chen, W.; Wong, M. W.; Andres, J. L.; Gonzalez, C.; Head-Gordon, M.; Replogle, E. S.; Pople, J. A. *Gaussian 98*, revision A.11.1; Gaussian, Inc.: Pittsburgh, PA, 2001.

(22) Bresgunov, A. Yu.; Dubinsky, A. A.; Poluektov, O. G.; Lebedev, Ya. S.; Prokof'ev, A. I. *Mol. Phys.* **1992**, *75*, 1123−1131.

(23) Ohya, H.; Yamauchi, J. *Electron spin resonance (in Japanese)*; Koudansha Scientific: Tokyo, 1989; p 114.

(24) The ESR simulation software is available free of charge via the Internet at http://www.bruker.com.